

# Random Complexes

MAA & JJP

May 8, 2008

## 1 Growing complexes

We build random two-dimensional complexes by growing and by bistellar swaps with functions we describe below. We are making a *Mathematica* package of these functions we will send you soon. This will be part of the manual.

Both the growing and swapping processes generate only valid triangulations of oriented surfaces without boundary. We are most interested in what the expectation value of the genus is as the number of vertices in the triangulation grows. Preliminary results obtained by growing have generated pdfs that look vaguely Poisson.

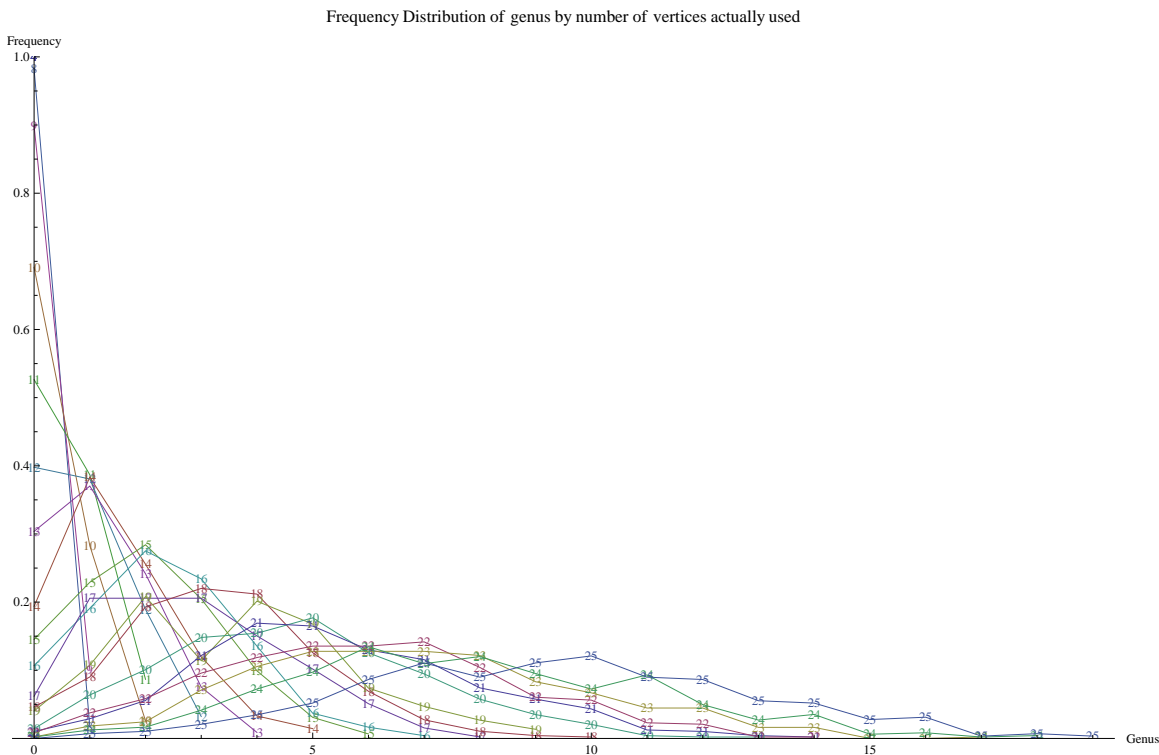


Figure 1: The relative frequencies of the occurrences of genera given vertex number, indicated by the plot marker on each curve.

The growing method aggregates simplices, starting from a single one  $C_0 = \{v[1], v[2], v[3]\}$ , to make a complex. At each stage  $n$ , a simplex is added to  $C_n$  by choosing an edge at random from  $\partial C_n$ , and suspending to a randomly chosen vertex  $v$  from  $\partial C_n$  or from outside  $C_n$ ,

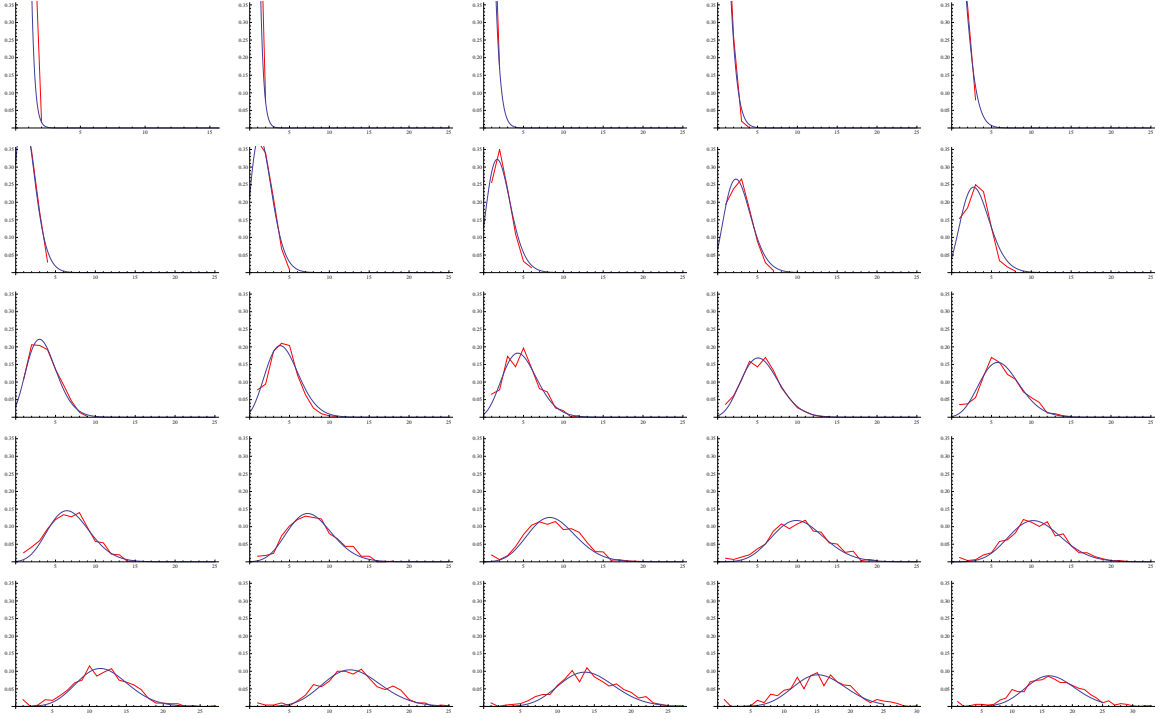


Figure 2: Same as previous figure with new data. The Poisson parameter  $\lambda$  goes quadratically with the number of vertices.

preserving orientation. For example, it could happen that

$$\begin{aligned}
 C_0 &= \{\{v[1], v[2], v[3]\}\} \rightsquigarrow \left( \underbrace{\{v[1], v[3]\}}_{\text{rand. from } \partial C_0}, \underbrace{v[5]}_{\text{rand. from univ}} \right) \\
 &\rightsquigarrow C_1 = \{\{v[1], v[2], v[3]\}, \underbrace{\{v[1], v[3], v[5]\}}_{\text{just added}}\} \rightsquigarrow \\
 &\rightsquigarrow \left( \underbrace{\{v[3], v[5]\}}_{\text{rand. from } \partial C_1 \text{ in } \partial C_0}, \underbrace{v[2]}_{\text{rand. from univ}} \right) \rightsquigarrow C_3 = \{\{v[1], v[2], v[3]\}, \underbrace{\{v[1], v[3], v[5]\}}_{\text{just added}}, \underbrace{\{v[2], v[5], v[3]\}}_{\text{just added}}\} \rightsquigarrow \dots
 \end{aligned}$$

As in the example, at each stage of growth, an edge  $e = \{v[k], v[l]\}$  is randomly chosen from  $\partial C_n$  and suspended to a vertex  $v[j]$  randomly chosen from  $\partial C_n$  or from universe vertices not already part of  $C_n$ . The successive complex  $C_{n+1}$  is obtained by adding the simplex  $\{v[j], v[k], v[l]\}$  to  $C_n$  in the order  $\{v[j], v[k], v[l]\}$  or  $\{v[j], v[l], v[k]\}$  that makes  $C_{n+1}$  oriented.

The complex  $C_n$  is required to be a valid pseudomanifold at every step, and growing is stopped when  $\partial C_n = 0$ .

For manifolds with a reasonable number of unique triangulations ( $\lesssim 200$ ), the growing method was shown to produce all of them within reasonable run length, suggesting that all triangulations are accessible via our method. Near the limit of our capabilities in finding triangulations, for a ten-vertex universe, growing 20000 complexes took about 2 hours. This run produced about 9000 ten-vertex spheres and produced 229 of the 233 of its triangulations. Binning these triangulations up to equivalence took about 9 hours. Both jobs were done on a 2.2 GHz MacBook running *Mathematica* 6.0.2.0.

Since the manifold may become boundaryless before all of the available vertices are used, complexes of various sizes are produced from a single run. For example, growing 54,000 complexes in a ten-vertex universe produced the following distribution of surfaces:

	Vertices used						
	4	5	6	7	8	9	10
<i>g=0</i>	1150	989	1095	1435	2668	6380	25179
<i>g=1</i>	0	0	0	2	42	679	13330
<i>g=2</i>	0	0	0	0	0	0	1042
<i>g=3</i>	0	0	0	0	0	0	9

We have noticed that the distribution of different types of manifolds is dependent on the number of vertices in the universe. Experiments are underway to make this dependence precise. An easier present goal than this is to experimentally estimate the prevalence of each distinct triangulation of a fixed manifold, *cf.* Lutz' table 1. We will refer to these systematically  $t_{g,v;j}$ , where  $g$  = genus,  $v$  = number of vertices, and  $j$  stands for the triangulation's place in our ordering. We will describe this later.

Table 1: Equivalence class count from Lutz (the less feasible ones are in italics).

vertices / genus	0	1	2	3	4	5	6
6	2	–	–	–	–	–	–
7	5	1	–	–	–	–	–
8	14	7	–	–	–	–	–
9	50	112	–	–	–	–	–
10	233	<i>2109</i>	<i>865</i>	20	–	–	–
11	<i>1249</i>	<i>37867</i>	<i>113506</i>	<i>65878</i>	<i>821</i>	–	–
12	<i>7595</i>	<i>605496</i>	<i>7085444</i>	<i>25608643</i>	<i>14846522</i>	<i>751593</i>	59

Although the size of the universe controls strongly what genera come out of growing, it seems that, when the data set is restricted to complexes of a fixed genus and number of vertices actually used, the distribution of the different triangulations is somewhat insensitive to the initial universe size (see for example Figs. 6 and 8). Below, we compare the prevalence of different triangulations achieved by random growing and by random bistellar swaps.

## 2 Examples and methods

Something you suggested was to consider occupation rates of triangulations under random bistellar moves. This has turned out to be very fruitful and we have been able to get a lot of data of this type. There seems to be little relation to the random growing process except at the extremes.

### 2.1 6-vertex spheres

Let the transition count matrix element  $m_{ij}$  be the number of ways the  $i^{th}$  triangulation class can be swapped into the  $j^{th}$  one—in short  $m_{ij} = \#(i \rightarrow j)$ . For bistellar swaps on

$(g, v) = (0, 6)$  (cf. Lutz' chart 1 above),  $m$  is

$$m = \begin{pmatrix} 4 & 1 \\ 12 & 0 \end{pmatrix}.$$

This means that the octahedron (class  $i = 2$ ) goes over to the double barycentric subdivision of the tetrahedron (dbst) (class  $i = 1$ ) in 12 distinct ways, one each for its 12 edges, while the dbst has four distinct swaps into itself and one that carries it to the octahedron. The zero in the 2,2 position means that the octahedron is never swapped into itself and so must go over to the dbst. Cf. the function `UnorderedCountMatrix` below.

Normalizing the rows of  $m$  and taking the transpose, we obtain the Markov transition matrix whose high powers converge to the stationary probability distribution,

$$\tilde{m}^n \longrightarrow \frac{1}{6} \begin{pmatrix} 5 & 5 \\ 1 & 1 \end{pmatrix}$$

indicating that the dbst  $\binom{1}{0}$  is 5 times as common as the octahedron  $\binom{0}{1}$ . This is called the *stationary probability distribution* (spd) of the chain.

The figure compares the results of growing in various sizes of vertex sets (we will call this a *universe size*) with the spd of the Markov chain.

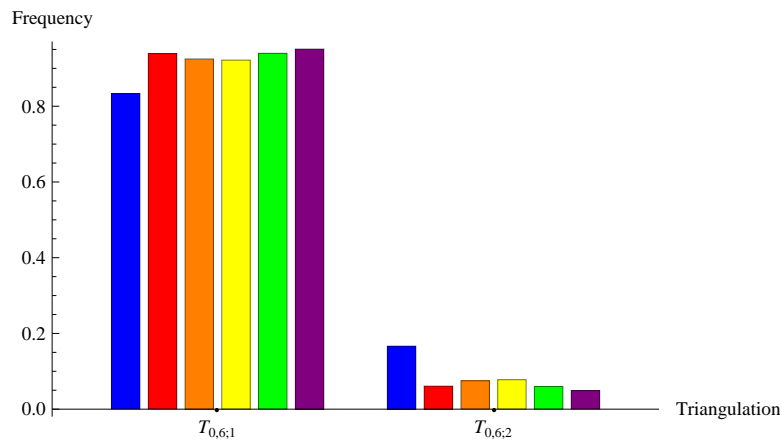


Figure 3: Histogram of spd (blue) and growth rates in universe sizes 10 (red), 9 (orange), 8 (yellow), 7 (green), 6 (purple) for 6-vertex spheres.

## 2.2 7-vertex spheres

The 7-vertex sphere has five equivalence classes of triangulations (described in Table 2). The count matrix is

$$m = \begin{pmatrix} 3 & 2 & 2 & 0 & 0 \\ 6 & 0 & 0 & 3 & 3 \\ 4 & 0 & 0 & 2 & 1 \\ 0 & 3 & 3 & 0 & 0 \\ 0 & 10 & 5 & 0 & 0 \end{pmatrix},$$

thus, for example  $t_{0,7;5}$  swaps to  $t_{0,7;2}$  in 10 ways as  $m_{52} = 10$ .

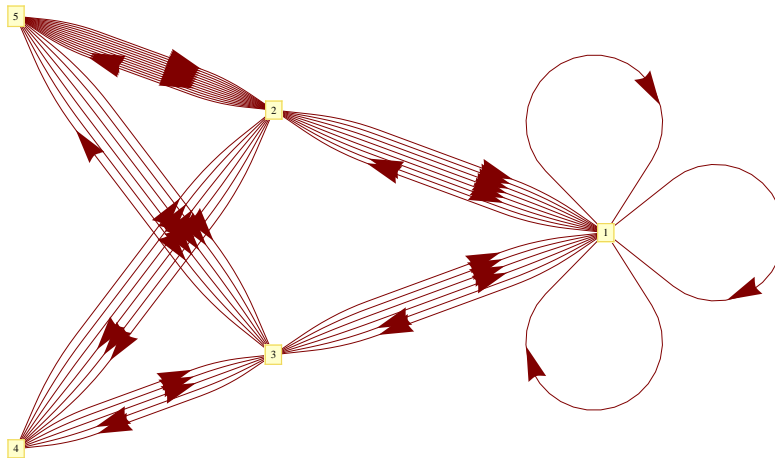


Figure 4: Connectivity graph of the counts matrix for 7-vertex spheres. As the graph is connected, we expect one spd. NB  $t_{0,7;5}$  is prime and so has many equivalent edges at which it can be swapped out (to  $t_{0,7;2}$  or  $t_{0,7;3}$ ). Its high symmetry is also related to the fact that there are only swaps out of  $t_{0,7;5}$  and few toward it, as is captured in the automorphism groups of the connectivity graphs. This is one “reason” why these high-symmetry primes are rare for swap ensembles.

The distributions of triangulations achieved by bistellar swaps and growing are shown in Table 2 and Fig. 6. The column headed *Markov prob* gives the stationary probability distribution (spd) of the process. In this case, the probabilities are equal to the single eigenvector of the transition matrix that can be interpreted as a list of probabilities.

A run of 10,000 sequential random swaps of a 7-vertex sphere yielded a population (column headed *Random swaps*) corresponding well to the spd of the transition matrix and giving us confidence that the random swaps are being adequately generated. Check that  $1926/10000 \approx 7/36, \dots$

The distribution of triangulations of 10,000 7-vertex spheres grown in a seven-vertex universe is shown in the column headed *Random growing*; this distribution is maintained when complexes are grown in universes of different sizes (Fig. 6). While the distributions of triangulations achieved by swapping and growing are not the same, there does seem to be a good correspondence between the most rare and the most common.

We are also studying lineages of triangulations under barycentric subdivision and possible relations of this property and commonality of occurrence of a triangulation. We call a triangulation that is not a barycentric subdivision of any other valid complex *prime*.

Another invariant of a triangulation is what we call its *valence profile*, the list of valences of the vertices. For small vertex sets, this is a useful tool for rapidly differentiating triangulations.

Table 2:  $(g,v)=(0,7)$

Name	Valence profile	Triangulation description <sup>a</sup>	Markov prob.	Random swaps (n=10,000)	Random growing <sup>b</sup> (n=10,000)
$t_{0,7;1}$	$\{3, 3, 4, 4, 5, 5, 6\}$	barycent subd of dbst at 9	7/18	3889	4974
$t_{0,7;2}$	$\{3, 4, 4, 4, 5, 5, 5\}$	barycent subd of octa	2/9	2217	988
$t_{0,7;3}$	$\{3, 3, 4, 4, 4, 6, 6\}$	barycent subd of dbst at 7	7/36	1926	2358
$t_{0,7;4}$	$\{3, 3, 3, 5, 5, 5, 6\}$	barycent subd of dbst at 8	1/9	1138	1476
$t_{0,7;5}$	$\{4, 4, 4, 4, 4, 5, 5\}$	prime	1/12	830	204

<sup>a</sup>See Fig 5

<sup>b</sup>Grown in a seven-vertex universe.

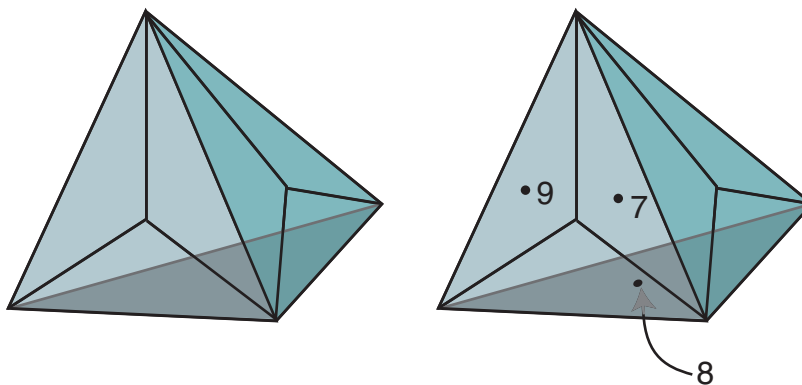


Figure 5: Diagram showing the dbst (left) and the positions of barycenters for its inequivalent subdivisions (right).

The connectedness of simplices  $s_k$  in a complex  $C$  of size  $n$  can be described by a pair of graphs on  $n$  vertices  $w_k$ :

$$C = \{s_1, s_2, \dots, s_n\} \mapsto G_1 = \{w_1, w_2, \dots, w_n \mid R_1\}, \quad G_2 = \{w_1, w_2, \dots, w_n \mid R_2\}$$

where  $R_1$  connects two nodes  $w_i$  and  $w_j$  iff  $s_i$  and  $s_j$  share only one vertex and where  $R_2$  connects two nodes  $w_i$  and  $w_j$  iff  $s_i$  and  $s_j$  share an edge. It is with these two graphs that the equivalence of triangulations is tested, via *Combinatorica*'s `IsomorphicQ` function, valid on graphs. Our function, which takes a complex, computes its graphs  $G_h$  ( $h = 1, 2$ ) as above and checks `IsomorphicQ` for them, is called `ComplexesEquivalentQ`.

We also examine the sizes of the groups of automorphisms of these graphs and have seen some (inverse) correlation between their sizes and the commonality of occurrence of a triangulation in growth (Figure 7). Curiously, this quantity better describes growth than bistellar swaps.

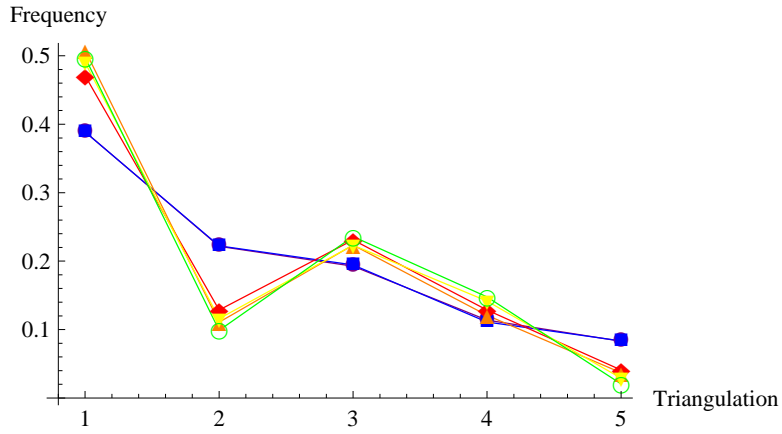


Figure 6: The relative frequencies of the occurrences of the five nonequivalent triangulations of the sphere on 7 vertices. These were generated by random bistellar swaps (purple) and random growing in universes of sizes 10 (red), 9 (orange), 8 (yellow), and 7 (green). The Markov spd is shown in blue. The horizontal axis tick marks represent the 5 equivalence classes of triangulations  $t_{0,7;1}, t_{0,7;2}, t_{0,7;3}, t_{0,7;4}, t_{0,7;5}$ .

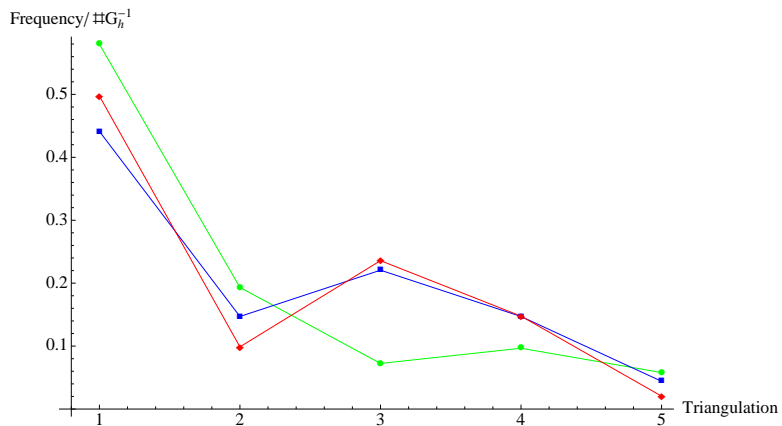


Figure 7: For  $h = 1$  (green), and  $h = 2$  (blue), we plot  $(\#G_h)^{-1}$  (normalized) versus the growth distribution (red) of 7-vertex spheres.

## 2.3 8-vertex spheres

For 8-vertex spheres, the count matrix for swaps is

$$m = \begin{pmatrix} 1 & 1 & 1 & 1 & 1 & 2 & 1 & 0 & 0 & 1 & 0 & 0 & 0 & 0 \\ 1 & 2 & 1 & 1 & 0 & 0 & 1 & 1 & 0 & 1 & 0 & 0 & 0 & 0 \\ 2 & 2 & 0 & 2 & 0 & 0 & 0 & 2 & 3 & 0 & 2 & 1 & 1 & 0 \\ 2 & 2 & 2 & 2 & 2 & 2 & 1 & 0 & 0 & 0 & 1 & 0 & 0 & 0 \\ 2 & 0 & 0 & 2 & 2 & 2 & 0 & 0 & 0 & 0 & 0 & 1 & 0 & 0 \\ 4 & 0 & 0 & 2 & 2 & 0 & 0 & 0 & 1 & 0 & 0 & 0 & 0 & 0 \\ 2 & 2 & 0 & 1 & 0 & 0 & 0 & 1 & 2 & 0 & 0 & 0 & 0 & 0 \\ 0 & 4 & 4 & 0 & 0 & 0 & 2 & 0 & 0 & 0 & 1 & 0 & 0 & 1 \\ 0 & 0 & 6 & 0 & 0 & 2 & 4 & 0 & 0 & 0 & 0 & 0 & 0 & 0 \\ 4 & 4 & 0 & 0 & 0 & 0 & 0 & 0 & 0 & 0 & 0 & 0 & 1 & 0 \\ 0 & 0 & 8 & 4 & 0 & 0 & 0 & 2 & 0 & 0 & 4 & 0 & 0 & 0 \\ 0 & 0 & 6 & 0 & 6 & 0 & 0 & 0 & 0 & 0 & 0 & 0 & 0 & 0 \\ 0 & 0 & 12 & 0 & 0 & 0 & 0 & 0 & 6 & 0 & 0 & 0 & 0 & 0 \\ 0 & 0 & 0 & 0 & 0 & 0 & 0 & 6 & 0 & 0 & 0 & 0 & 0 & 0 \end{pmatrix}$$

and the stationary probability distribution is  $\left\{ \frac{3}{19}, \frac{8}{57}, \frac{5}{38}, \frac{7}{57}, \frac{3}{38}, \frac{3}{38}, \frac{4}{57}, \frac{1}{19}, \frac{1}{19}, \frac{3}{76}, \frac{3}{76}, \frac{1}{57}, \frac{1}{76}, \frac{1}{228} \right\}$ .

Here we gather data regarding our growing of these spheres.

Table 3:  $(g,v)=(0,8)$

Name	Valence profile	Triangulation description <sup>a</sup>	Markov prob.	Random growing <sup>b</sup> (n=10,000)
$t_{0,8;1}$	{3, 3, 4, 4, 4, 5, 6, 7}	gen-2 descendant of the dbst	3/19	2198
$t_{0,8;2}$	{3, 3, 3, 4, 5, 5, 6, 7}	gen-2 descendant of the dbst	8/57	2027
$t_{0,8;3}$	{3, 4, 4, 4, 5, 5, 5, 6}	subd of $t_{0,7;5}$ (which is prime)	5/38	437
$t_{0,8;4}$	{3, 4, 4, 4, 4, 5, 6, 6}	gen-2 descendant of the octahedron	7/57	728
$t_{0,8;5}$	{3, 3, 4, 4, 5, 5, 6, 6}	gen-2 descendant of the dbst	3/38	1144
$t_{0,8;6}$	{3, 3, 4, 4, 5, 5, 5, 7}	gen-2 descendant of the dbst	3/38	1059
$t_{0,8;7}$	{3, 3, 3, 4, 5, 6, 6, 6}	gen-2 descendant of the dbst	4/57	1004
$t_{0,8;8}$	{3, 3, 4, 4, 5, 5, 6, 6}	gen-2 descendant of the octahedron	1/19	317
$t_{0,8;9}$	{3, 3, 4, 5, 5, 5, 5, 6}	gen-2 descendant of the octahedron	1/19	294
$t_{0,8;10}$	{3, 3, 4, 4, 4, 4, 7, 7}	gen-2 descendant of the dbst	3/76	517
$t_{0,8;11}$	{4, 4, 4, 4, 5, 5, 5, 5}	prime	3/76	71
$t_{0,8;12}$	{3, 3, 5, 5, 5, 5, 5, 5}	gen-2 descendant of the octahedron	1/57	109
$t_{0,8;13}$	{4, 4, 4, 4, 4, 4, 6, 6}	prime	1/76	39
$t_{0,8;14}$	{3, 3, 3, 3, 6, 6, 6, 6}	gen-2 descendant of the dbst	1/228	56

<sup>a</sup>From Fig. 10

<sup>b</sup>Grown in an eight-vertex universe.

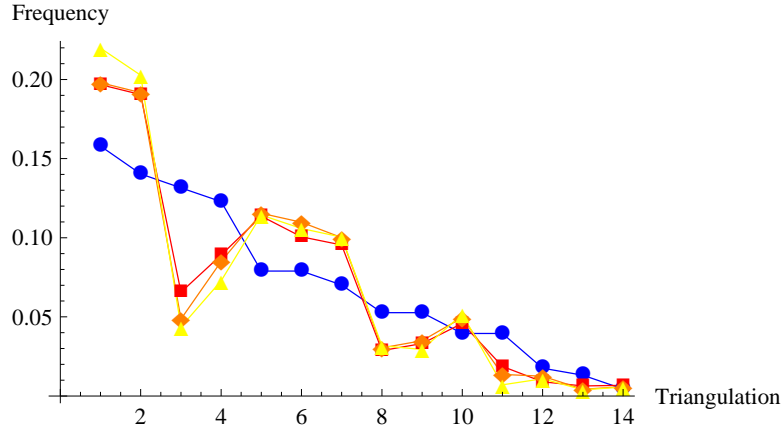


Figure 8: The relative frequencies of the occurrences of the fourteen nonequivalent triangulations of the sphere on 8 vertices. The Markov probabilities are shown in blue and the distributions from growing in 10-, 9-, and 8-vertex universes are shown in red, orange, and yellow, respectively. The horizontal axis tick marks represent the equivalence classes  $t_{0,8;1}, \dots, t_{0,8;14}$ .

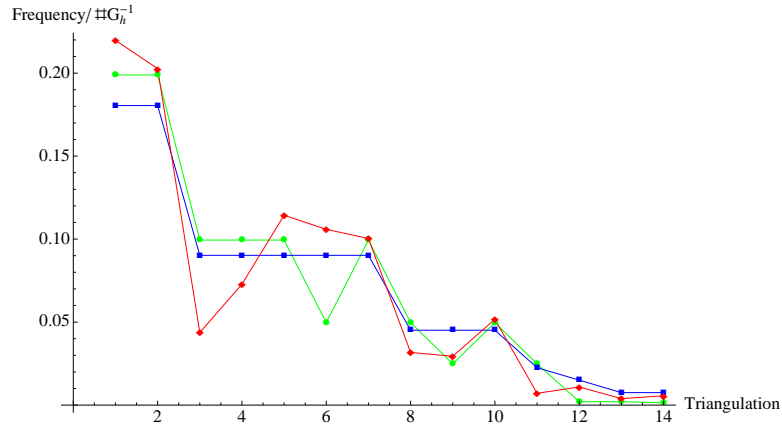


Figure 9: For  $h = 1$  (green), and  $h = 2$  (blue), we plot  $(\#G_h)^{-1}$  (normalized) versus the growth distribution (red) for 8-vertex spheres.

## 2.4 8-vertex 1-tori

Referring back to Lutz 1, we have 7 equivalence classes of triangulations (*cf.* 8.2). The count matrix is

$$m = \begin{pmatrix} 0 & 4 & 2 & 0 & 2 & 0 & 0 \\ 4 & 0 & 0 & 1 & 0 & 2 & 0 \\ 4 & 0 & 0 & 2 & 0 & 0 & 1 \\ 0 & 2 & 2 & 0 & 2 & 0 & 0 \\ 6 & 0 & 0 & 3 & 0 & 0 & 0 \\ 0 & 3 & 0 & 0 & 0 & 0 & 0 \\ 0 & 0 & 8 & 0 & 0 & 0 & 0 \end{pmatrix}.$$

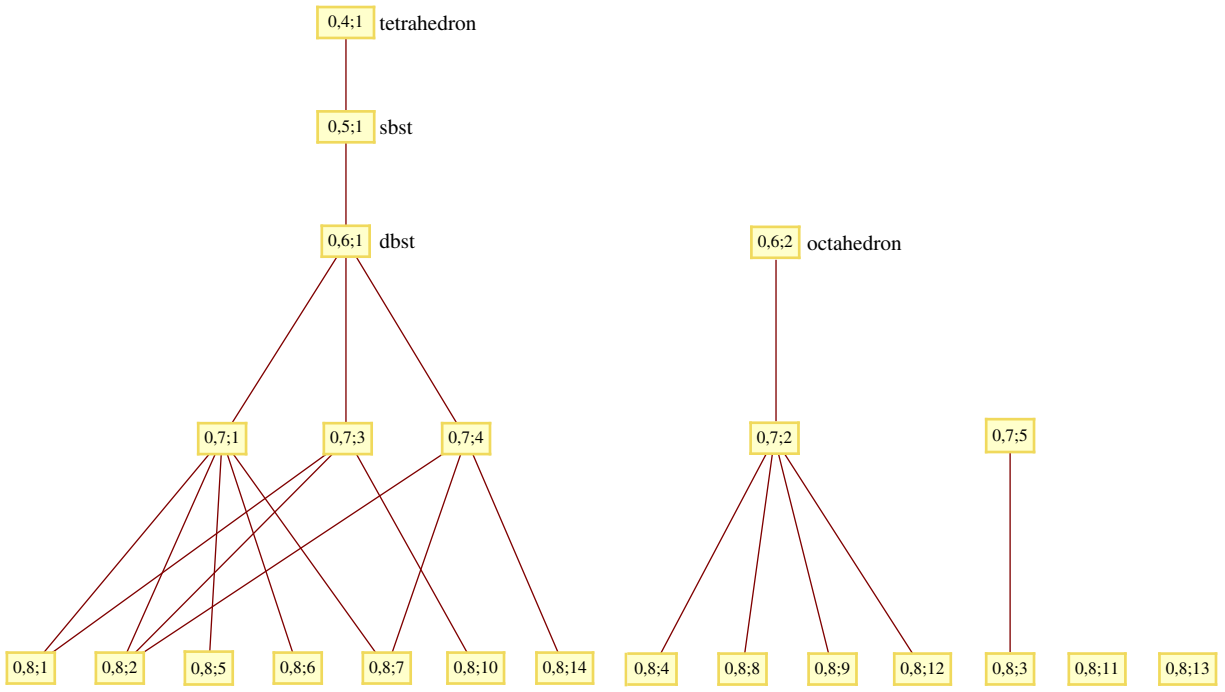


Figure 10: The genealogy of the 8-vertex sphere by barycentric subdivision. The triangulations are labeled  $t_{0,8;1} \rightarrow 0, 8; 1$ . NB  $t_{0,8;11}$  and  $t_{0,8;13}$  are prime.

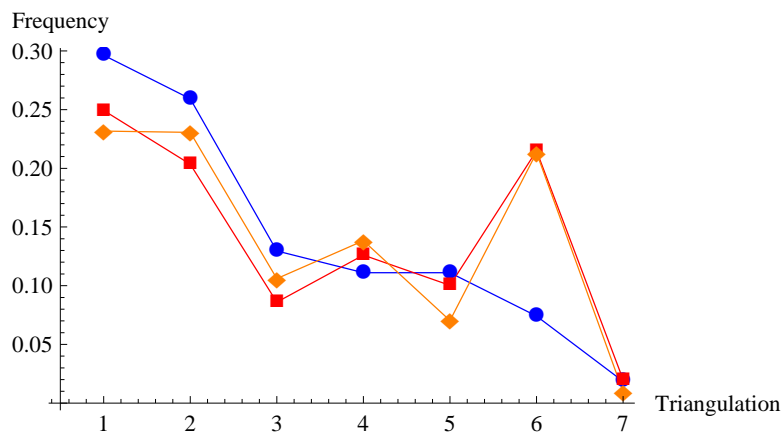


Figure 11: The relative frequencies of the occurrences of the 7 nonequivalent triangulations of the 8-vertex 1-torus. The Markov probabilities are shown in blue and the distributions from growing in 9-, and 8-vertex universes are shown in red and orange. The horizontal axis tick marks represent the equivalence classes  $t_{1,8;1}, \dots, t_{1,8;7}$ .

Table 4:  $(g,v)=(1,8)$

Name	Valence profile <sup>a</sup>	Triangulation description	Markov prob.	Random growing <sup>b</sup> n=3000
$t_{1,8;1}$	$\{5, 5, 6, 6, 6, 6, 7, 7\}$	prime	8/27	695
$t_{1,8;2}$	$\{4, 6, 6, 6, 6, 6, 7, 7\}$	prime	7/27	692
$t_{1,8;3}$	$\{5, 5, 6, 6, 6, 6, 7, 7\}$	prime	7/54	318
$t_{1,8;4}$	$\{4, 5, 5, 6, 7, 7, 7, 7\}$	prime	1/9	415
$t_{1,8;5}$	$\{5, 5, 5, 6, 6, 7, 7, 7\}$	prime	1/9	211
$t_{1,8;6}$	$\{3, 6, 6, 6, 6, 7, 7, 7\}$	barycent subd of (1,7)	2/27	640
$t_{1,8;7}$	$\{6, 6, 6, 6, 6, 6, 6, 6\}$	prime	1/54	29

<sup>a</sup>Notice that  $t_{1,8;1}$  and  $t_{1,8;3}$  have the same vertex valence profile, although they are distinct triangulations.

<sup>b</sup>Grown in an eight-vertex universe.

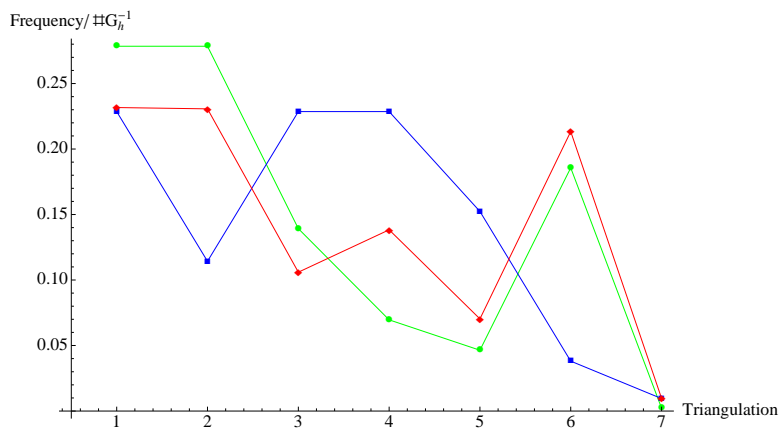


Figure 12: For  $h = 1$  (green), and  $h = 2$  (blue), we plot  $(\#G_h)^{-1}$  (normalized) versus the growth distribution (red) for 8-vertex 1-tori.

## 2.5 9-vertex spheres

The spd is

$$\left\{ \frac{1}{506}, \frac{7}{1518}, \frac{7}{1518}, \frac{4}{759}, \frac{3}{506}, \frac{1}{138}, \frac{5}{506}, \frac{8}{759}, \frac{3}{253}, \frac{10}{759}, \frac{10}{759}, \frac{10}{759}, \frac{10}{759}, \frac{7}{506}, \frac{7}{506}, \frac{1}{69}, \frac{1}{69}, \frac{1}{69}, \frac{1}{69}, \frac{1}{69}, \frac{4}{253}, \frac{4}{253}, \frac{14}{759}, \frac{14}{759}, \frac{14}{759}, \frac{5}{253}, \frac{5}{253}, \right. \\ \left. \frac{5}{253}, \frac{5}{253}, \frac{5}{253}, \frac{16}{759}, \frac{17}{759}, \frac{6}{253}, \frac{6}{253}, \frac{20}{759}, \frac{20}{759}, \frac{20}{759}, \frac{20}{759}, \frac{20}{759}, \frac{20}{759}, \frac{20}{759}, \frac{2}{69}, \frac{2}{69}, \frac{2}{69}, \frac{2}{69}, \frac{28}{759}, \frac{28}{759}, \frac{32}{759}, \frac{34}{759}, \frac{12}{253} \right\}.$$

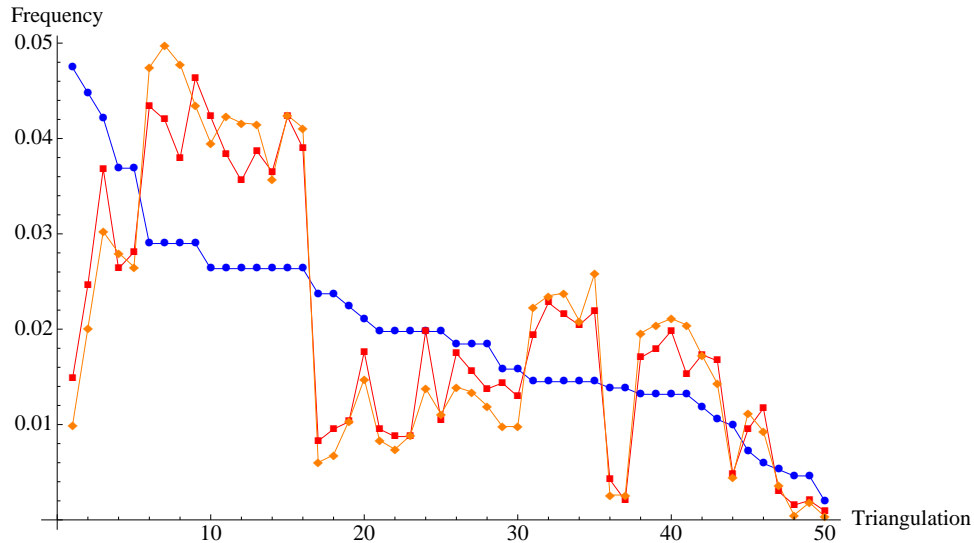


Figure 13: The relative frequencies of the occurrences of the 50 nonequivalent triangulations of the 9-vertex sphere. The Markov probabilities are shown in blue and the distributions from growing in 10-, and 9-vertex universes are shown in red and orange. The horizontal axis tick marks represent the equivalence classes  $t_{0,9;1}, \dots, t_{0,9;50}$ .

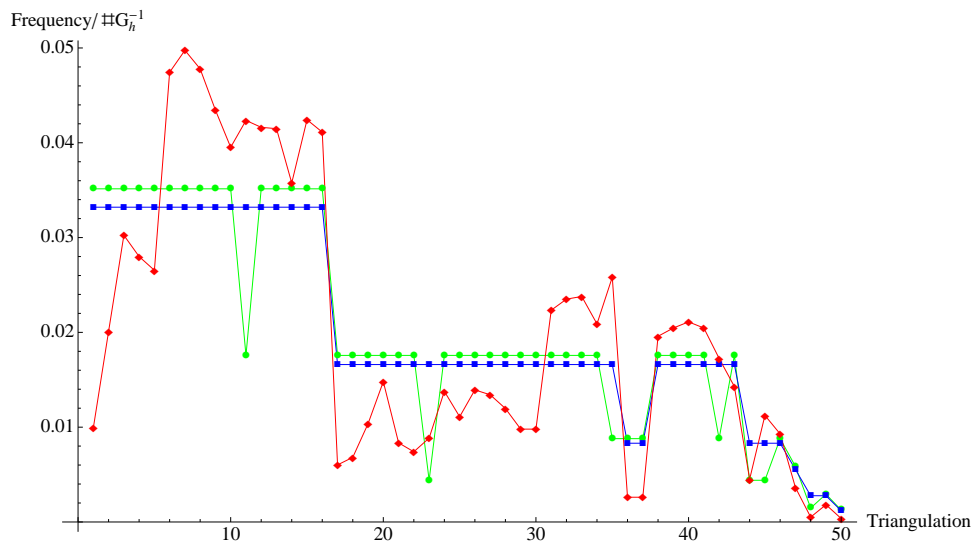


Figure 14: For  $h = 1$  (green), and  $h = 2$  (blue), we plot  $(\#G_h)^{-1}$  (normalized) versus the growth distribution (red) for 9-vertex spheres.

## 2.6 9-vertex 1-tori

The list of probs:

$$\left\{ \frac{17}{894}, \frac{8}{447}, \frac{5}{298}, \frac{5}{298}, \frac{5}{298}, \frac{7}{447}, \frac{7}{447}, \frac{7}{447}, \frac{7}{447}, \frac{7}{447}, \frac{7}{447}, \frac{7}{447}, \frac{13}{894}, \frac{13}{894}, \frac{13}{894}, \frac{2}{149}, \frac{2}{149}, \frac{2}{149}, \frac{2}{149}, \frac{2}{149}, \frac{2}{149}, \frac{2}{149}, \frac{2}{149}, \frac{11}{894}, \frac{11}{894}, \frac{11}{894}, \frac{11}{894}, \frac{11}{894}, \right.$$

$$\frac{11}{894}, \frac{11}{894}, \frac{11}{894}, \frac{5}{447}, \frac{5}{447}, \frac{5}{447}, \frac{5}{447}, \frac{5}{447}, \frac{5}{447}, \frac{5}{447}, \frac{5}{447}, \frac{3}{298}, \frac{3}{298}, \frac{3}{298}, \frac{3}{298}, \frac{3}{298}, \frac{3}{298}, \frac{3}{298}, \frac{3}{298}, \frac{3}{298}, \frac{17}{1788}, \frac{4}{447}, \frac{4}{447}, \frac{4}{447}, \frac{4}{447}, \frac{4}{447},$$

$$\frac{4}{447}, \frac{5}{596}, \frac{5}{596}, \frac{5}{596}, \frac{5}{596}, \frac{5}{596}, \frac{5}{596}, \frac{7}{894}, \frac{7}{894}, \frac{7}{894}, \frac{13}{1788}, \frac{13}{1788}, \frac{13}{1788}, \frac{13}{1788}, \frac{13}{1788}, \frac{13}{1788}, \frac{13}{1788}, \frac{1}{149}, \frac{1}{149}, \frac{1}{149}, \frac{1}{149}, \frac{1}{149}, \frac{1}{149}, \frac{1}{149}, \frac{1}{149}, \frac{1}{149}, \frac{11}{1788},$$

$$\frac{11}{1788}, \frac{7}{1192}, \frac{5}{894}, \frac{5}{894}, \frac{5}{894}, \frac{5}{894}, \frac{5}{894}, \frac{5}{894}, \frac{3}{596}, \frac{3}{596}, \frac{3}{596}, \frac{3}{596}, \frac{3}{596}, \frac{2}{447}, \frac{2}{447}, \frac{2}{447}, \frac{2}{447}, \frac{5}{1192}, \frac{5}{1192}, \frac{5}{1192}, \frac{5}{1192}, \frac{13}{3576}, \frac{1}{298}, \frac{5}{1788}, \frac{3}{1192},$$

$$\left. \frac{1}{447}, \frac{1}{894}, \frac{1}{894}, \frac{1}{1192}, \frac{1}{1192}, \frac{1}{3576} \right\}$$

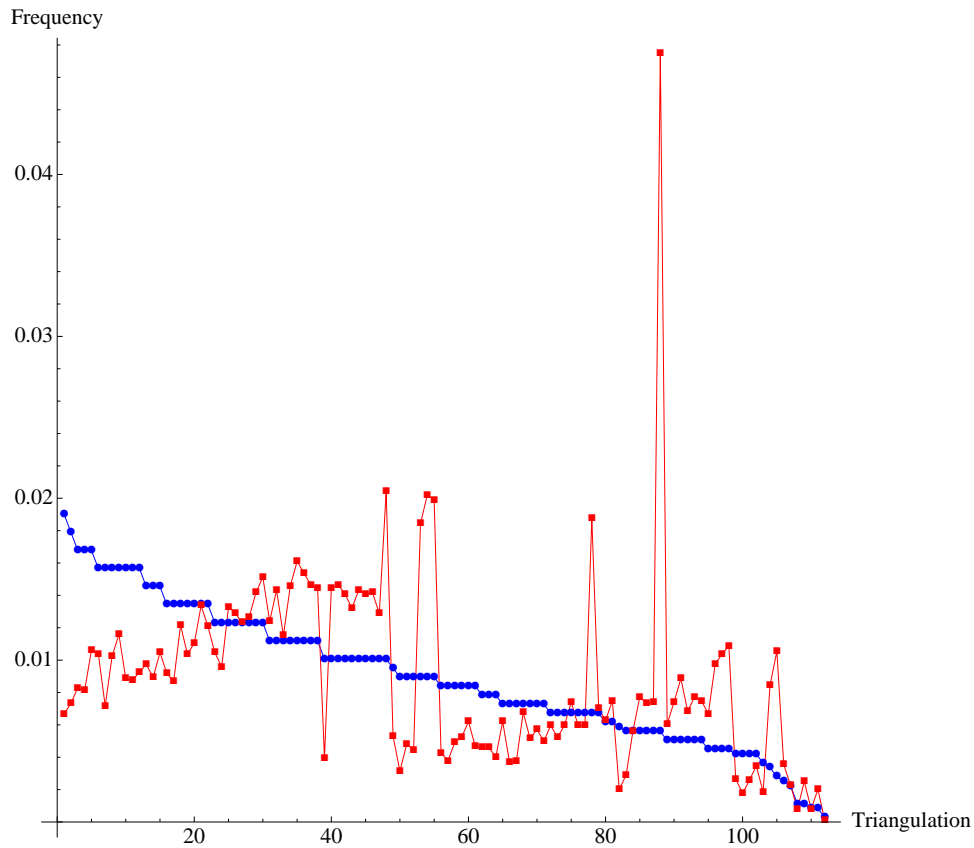


Figure 15: The relative frequencies of the occurrences of the 112 nonequivalent triangulations of the torus on 9 vertices. The Markov probabilities are shown in blue and the distributions from growing in a 9-vertex universe is shown in red. The horizontal axis tick marks represent the equivalence classes  $t_{0,9;1}, \dots, t_{0,9;112}$ .



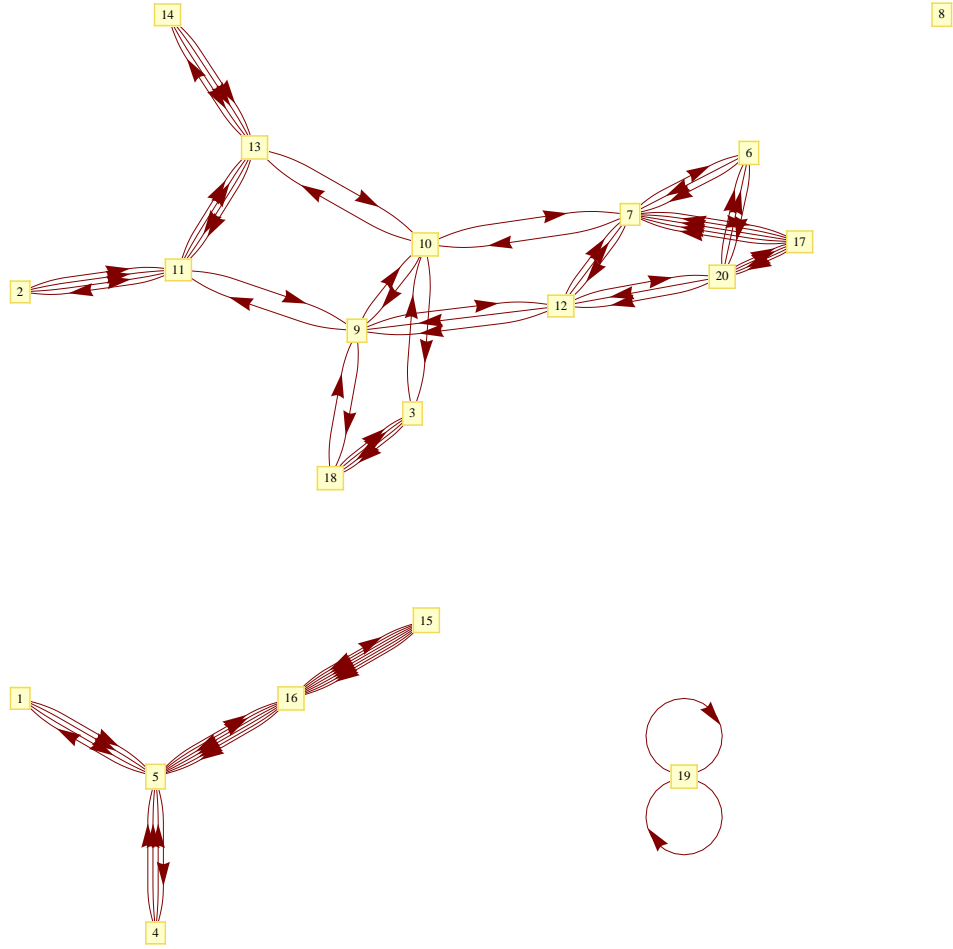


Figure 16: Graph representation of the connectivity of triangulations of the ten-vertex 3-torus under bistellar swaps. Since this graph is not connected, there is more than one spd.



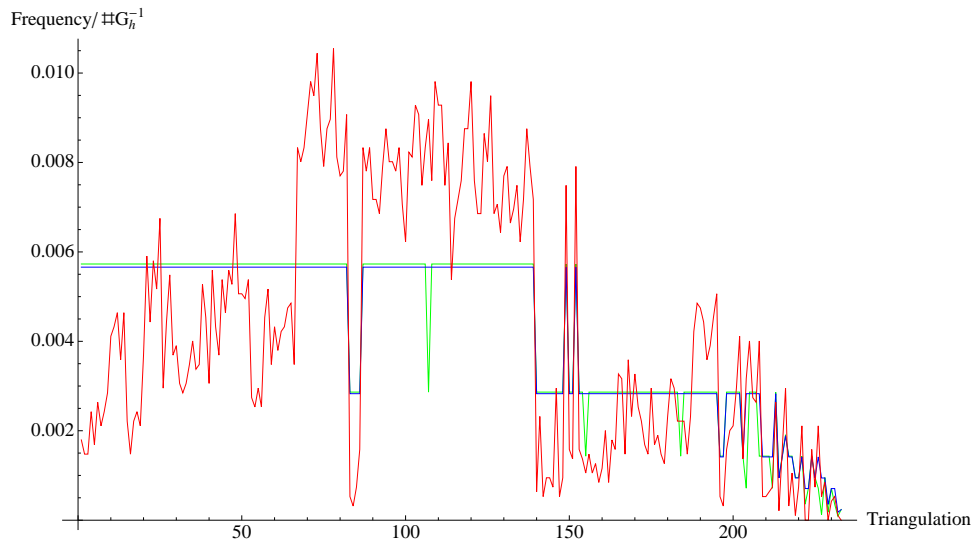


Figure 18: For  $h = 1$  (green), and  $h = 2$  (blue), we plot  $(\#G_h)^{-1}$  (normalized) versus the growth distribution (red) for 10-vertex spheres.

### 3 12-vertex 6-tori

Interesting: The counts matrix gave a totally disconnected graph:

$$m = 0.$$

### 4 Contrast between growth and swaps

Inasmuch as there is some dependence on growth universe, bistellar swaps and growing must be different.

Still, the minimum frequencies occur at a triangulations that are not a barycentric subdivision of any other for growth as well as for swaps.

## 5 Brooks and Makover

In the paper [BM], Brooks and Makover parametrize triangulations of Riemann surfaces by 3-regular graphs with orientations. Here we quote:

Let  $\Gamma$  be a finite 3-regular graph. We will allow  $\Gamma$  to contain loops and multiple edges. An orientation  $\mathcal{O}$  on the graph is the assignment, for each vertex  $v$  of  $\Gamma$ , of a cyclic ordering of the three edges emanating from  $v$ . If  $\Gamma$  has  $2n$  vertices, then clearly there are  $2^{2n}$  orientations on  $\Gamma$ .

Also,

We may now construct the surface  $S^{\mathcal{O}}(\Gamma, \mathcal{O})$  from  $(\Gamma, \mathcal{O})$  by placing on each vertex  $v$  of  $\Gamma$  a copy of  $T$  [a triangle with edges marked with midpoints], so that the cyclic ordering of the segments in  $T$  agrees with the orientation at the vertex  $v$  in  $\Gamma$ . If two vertices of  $\Gamma$  are joined by an edge, we glue the two copies of  $T$  along the corresponding sides subject to the following two conditions: (a) the midpoints of the two sides are glued together, and (b) the gluing preserves the orientation of the two copies of  $T$ . The conditions (a) and (b) determine the gluing uniquely.

A reasonable goal here is to understand how our growing behavior relates to Brooks': Their relevant result is that if  $S^c$  is the *conformal compactification* of  $S^{\mathcal{O}}$ ,

*Theorem 2.3. There exist constants  $C_1$  and  $C_2$  such that the expected value of the genus  $\text{genus}(S^c(\Gamma, \mathcal{O}))$ , where  $(\Gamma, \mathcal{O})$  is randomly selected among oriented 3-regular graphs on  $2n$  vertices, satisfies*

$$1 + n/2 - \left[ C_1 + \frac{3 \log(n)}{4} \right] \leq \mathbb{E}(\text{genus}(S^c(\Gamma, \mathcal{O}))) \leq 1 + n/2 - \left[ C_2 + \frac{\log(n)}{2} \right].$$

We begin by setting some notation. First, the physical triangulation as grown randomly before will continue to be written, *e.g.*

$$C = \{ \{v[1], v[2], v[3]\}, \{v[1], v[3], v[5]\}, \{v[2], v[5], v[3]\}, \dots \}.$$

Note that as the vertices of  $\{v[x], v[y], v[z]\}$  are labeled so that the orientation is expressed by the equivalences

$$\{v[x], v[y], v[z]\} \sim \{v[z], v[x], v[y]\} \sim \{v[y], v[z], v[x]\}.$$

In this notation there is no doubt as to the number of vertices, edges, or triangles present so it is obvious how to compute the Euler characteristic of the complex.

In [BM], the situation is similar. The description of the triangulation is in terms of a graph for which each of the vertices has an orientation associated. We provide a translation between the two methods of describing the triangulation:

The list of vertices,  $\beta_1, \beta_2, \beta_3, \dots$ , of [BM]'s 3-regular graph, will correspond to our triangles

$$\beta_j \longleftrightarrow \{v[x_j], v[y_j], v[z_j]\}.$$

Note that lacking orientations, the list of vertices  $\beta_1, \beta_2, \beta_3, \dots$  does not provide all the information needed to build the complex. Thus, each of these vertices must be given a cyclic ordering of the edges emanating from it. [BM] do not delineate this procedure explicitly, so we will come up with our own recipe.

Let  $\Gamma$  be the 3-regular graph on vertices  $\{\beta_1, \beta_2, \beta_3, \dots, \beta_\nu\}$  with edges  $E = \{e_{ij} \mid i, j = 1, \dots, \nu\}$  so that  $\beta_i, \beta_j$  have edge(s)  $e_{ij}$  connecting them. NB double edges are permitted so  $E$  can have repeated elements. The orientation at the vertex  $\beta_i$  we express by groupings (like those of  $\{v[x], v[y], v[z]\}$ ) of the edges emanating from  $\beta_j$ ,  $\{e_{ij}, e_{ik}, e_{il}\}$  where, as before

$$\{e_{ij}, e_{ik}, e_{il}\} \sim \{e_{il}, e_{ij}, e_{ik}\} \sim \{e_{ik}, e_{il}, e_{ij}\}$$

Again, note that  $j, k, l$  need not all be distinct.

This suggests we write the graph with orientation  $(\Gamma, \mathcal{O})$  in the following form:

$$rep(\Gamma, \mathcal{O}) = \{\{e_{ij}, e_{ik}, e_{il}\}, \{e_{i'j'}, e_{i'k'}, e_{i'l'}\}, \{e_{i''j''}, e_{i''k''}, e_{i''l''}\}, \dots\}$$

where just as above, it is understood that the  $\beta_i$  for which  $i$  is an index in  $(\Gamma, \mathcal{O})$  are the vertices. The edges  $\{e_{ij}, e_{ik}, e_{il}\}$  are those emanating from vertex  $\beta_i$  and Brooks and Makover's idea of the left-hand turn becomes then going to the next edge in a triplet in  $rep(\Gamma, \mathcal{O})$ . A typical left-hand turn:

$$rep(\Gamma, \mathcal{O}) = \{\dots, \underbrace{\{e_{ij}, e_{ik}, e_{il}\}}_{\beta_i}, \dots, \underbrace{\{e_{ki}, e_{km}, e_{kn}\}}_{\beta_k}, \dots\}, \quad LHT : e_{ik} \mapsto e_{km}.$$

Considering the vertices  $\beta_i$  as if they were points at the centers of the triangles  $\{v[x], v[y], v[z]\}$ , the edges  $\{v[x], v[y]\}, \{v[y], v[z]\}, \{v[x], v[z]\}, \dots$  of  $C$  and the edges  $e_{ij}$  of  $(\Gamma, \mathcal{O})$  will each intersect one of the others exactly once. Thus they are in one-to-one correspondence.

To get topological data, we again go to [BM]:

Definition 4.1. A left-hand-turn path (for short, *LHT* path) on  $(\Gamma, \mathcal{O})$  is a closed path on  $\Gamma$  such that, at each vertex, the path turns left in the orientation  $\mathcal{O}$ . Traveling on a path on  $\Gamma$  which always turns left describes a path on  $S^\mathcal{O}(\Gamma, \mathcal{O})$  which travels around a cusp. Indeed, if we set  $LHT = LHT(\Gamma, \mathcal{O})$  to be the number of disjoint left-hand-turn paths, then the topology of  $S^\mathcal{O}(\Gamma, \mathcal{O})$  is easily describable in terms of *LHT* and  $n$ , where again  $2n$  is the number of vertices in  $\Gamma$ . Indeed, the graph  $\Gamma$  divides  $S^\mathcal{O}(\Gamma, \mathcal{O})$  into *LHT* regions, each bordered by a left-hand-turn path and containing one cusp in its interior. From this, we can immediately read off the signature of  $S^\mathcal{O}(\Gamma, \mathcal{O})$  by the Euler characteristic. The genus of  $S^\mathcal{O}(\Gamma, \mathcal{O})$  is given by

$$genus = 1 + \frac{n - LHT}{2}$$

and the number of cusps is *LHT*. Note that the usual orientation on the 3-regular graph which is the 1-skeleton of the cube contains six left-hand-turn paths, giving that the associated surface is a sphere with six punctures, while a choice of a different orientation on this graph can have either two, four, or six left-hand-turn paths, so that the associated surface can have genus 0, 1, or 2.

The way they think of random graphs is as follows:

For each  $n$ , let  $\mathcal{F}_n$  denote the finite set of 3-regular graphs on  $2n$  vertices. We put a probability measure on  $\mathcal{F}_n$  in the following way: We consider a hat with  $6n$  balls, labeled by the integers  $1, 2, \dots, (2n)$ , with three copies of each number occurring. We begin with a graph consisting only of vertices labeled with the integers  $1, \dots, (2n)$ . We then add edges to the graph at random by selecting pairs of balls from the hat, without replacement. If at step  $i$  the integers  $l_i$  and  $m_i$  are selected, we add to the graph an edge joining  $l_i$  and  $m_i$ . We modify this picture to handle orientations in the following manner: We distinguish between the three balls with the same number by adding one of the letters  $a, b$ , and  $c$ . Thus, the balls are labeled  $1a, 1b, 1c, \dots, (2n)a, (2n)b, (2n)c$ . We denote the set of draws from this collection by  $\mathcal{F}_n^*$ . In this way, the three edges from vertex  $i$  are labeled by one of the letters  $\{a, b, c\}$ . We may then put a cyclic ordering on these edges by the cyclic ordering  $(a, b, c)$ . Thus, the probability measure on  $\mathcal{F}_n^*$  gives us a probability measure on the set of oriented 3-regular graphs  $(\Gamma, \mathcal{O})$  on  $2n$  vertices.

## 6 Functions

Our functions take and generate complexes expressed as in the following example: The tetrahedron is written

$$t = \{\{v[1], v[2], v[3]\}, \{v[1], v[3], v[4]\}, \{v[1], v[4], v[2]\}, \{v[2], v[4], v[3]\}\}.$$

Notice that we are careful about ordering as we will need to be building and operating on predictably orientable surfaces. We have a function `ValidateLutz` which takes a complex in the form that Lutz gives them (*i.e.* not respecting orientation) and outputs a valid complex.

Examples of functions:

$$\text{BoundaryMap}[t] = v[2] ** v[3] - v[1] ** v[3] + v[1] ** v[2]$$

$$+ v[3] ** v[4] - v[1] ** v[4] + v[1] ** v[3] + v[3] ** v[1] + \dots = 0,$$

where `**` is a noncommutative multiplication and we have a rule  $a ** b = -b ** a$ .

We have a function `ComplexesEquivalentQ` that determines whether two complexes are equivalent. A function `MakeAnnotatedBins` takes a run and outputs annotated bins. It sorts the complexes in a run up to equivalence and puts populations next to an example of the class.

The data structure called the *annotated bin* has the form

$$\{\{complex_1, population_1\}, \{complex_2, population_2\}, \dots, \{complex_n, population_n\}\}$$

where the population is that of the complex grouped alongside. We will call the complex in bin  $\{complex_i, population_i\}$  an *exemplar*.

I briefly and imprecisely describe our other main functions below.

The function `BoundaryMapMatrixRepresentation` takes the boundary map of a complex and writes its matrix representation in a basis of vectors from the one-skeleton.

`BettiOne` computes the first Betti number of the complex.

`BettiTwoSurfaces` computes the second Betti number for surfaces.

`EulerCharacteristic` computes the Euler characteristic of the complex and `Genus` computes the genus from the Euler characteristic.

`ValidComplexQ` determines whether a surface is valid as a pseudomanifold surface.

`ValidateLutz` takes an unordered complex and orders it so that it is written respecting the orientation of the first simplex. (This only makes sense for orientable surfaces.)

`SubComplex` takes  $(vertex, complex)$  and gives the subcomplex containing the vertex.

`GraphCutPointQ` takes a vertex in a complex and forms the one-skeleton of the subcomplex containing that vertex. It then determines whether the vertex disconnects this graph. If so, this vertex is a pinch point for the manifold constructed to this point and should be capped off (see below).

`BowTieQ` goes through all the vertices in a complex to determine whether any is a cut point as in the previous function. If there is, then the next function is called.

**CapBowTie** corrects a pinch point as above by adding another simplex to fatten it. If this is not possible, it deletes the problem. **EdgeInTriangleQ** and **EdgeOpenQ** are similarly checks for validity of the addition of a simplex to a complex.

**RandomComplexes** is the do-all function for randomly growing surfaces. It looks in the boundary at random for edges on which to add another simplex, either by suspending to a vertex in the universe or by suspending on another boundary vertex. It checks the validity of what it's added and starts over if it has broken a rule. If it has formed a pinch point, it calls **CapBowTie** to cap it off. It runs until the boundary is zero.

**SkeletonGraph** takes a complex and 1 or 2 and forms the graph of the connections of the simplices either sharing a vertex (1) or an edge (2).

**ComplexesEquivalentQ** determines whether two complexes are equivalent by checking whether their connectivity graphs at the level of vertices and edges are isomorphic.

**ValenceProfile** computes a weak invariant of a triangulation, the list of valences of its vertices.

**VertexValenceEquivalentQ** on two complexes determines whether the valence profiles of the two match.

**MakeAnnotatedBins** takes a list of complexes (e.g. randomly generated) and bins them according to their equivalence class, as triangulations.

**AppendToAnnotatedBins** we use to accumulate new data (lists of complexes) to old data so as to keep track of the equivalence classes of the triangulations.

**CorrespondBins** is another tool for accumulating differently labelled data. Adjoins new population data.

**BinAccordingToList** bins in the order determined by another list. Similar to **CorrespondBins**.

**SortAnnotatedBinsByDecreasingPopulation** does just that.

**RandomDiagSwap** generates a random bistellar swap on a complex and verifies that it has made a valid complex.

**RandomSwapEnsemble** makes sets of random swaps of complexes.

**DiagSwapAtKthEdgemeet** takes a complex and an integer  $k$ . It generates a list of pairs of simplices meeting on an edge and does a bistellar swap at the  $k^{th}$  of these. This function does *not* determine whether the complex it has produced is a valid two-manifold.

**UnnormalizedSwapMarkov** calls the previous function at all edge meetings of the simplices. It checks validity of the output of the diagonal swap and identifies the result up to equivalence of triangulation. It forms then a matrix  $(m_{ij})_{ij}$  where  $m_{ij}$  is the number of ways the  $i^{th}$  triangulation class can be swapped into the  $j^{th}$  one.

**NormalizeRowsAndTranspose**: The Markov transition matrix is constructed from the output of the previous function. This amounts to normalizing rows and taking the transpose.

**MarkovComponent** is a quick function for experiments. It takes a complex and  $(i, j)$  to give  $m_{ij}$  as above.

**PermMatrices** takes a permutation  $\sigma$  in the form  $\{\sigma(1), \sigma(2), \dots, \sigma(n)\}$  and outputs the usual matrix representation of  $\sigma$ .

`MakeDictionary` takes an annotated bin of triangulations and sorts it according to the Markov swap probability of the triangulation, going from most frequent to least frequent. Returns a list of lists of the form {exemplar complex, original position of the complex in the annotated bins, unnormalized Markov frequency}. The Markov frequencies are not normalized. Output of this form is called a *dictionary bin*.

`DictionaryToPermMatrix` takes a dictionary bin and writes the permutation matrix that reorders the bin to the order of the dictionary.

`OrderedCountMatrix` and `OrderedMarkovMatrix` generate the count matrix and the transition matrix with the bases ordered according to the Markov probabilities.

`SizeOfAutomorphismGroups` computes the number of automorphisms the skeleton graph of a complex has. The idea is that a large automorphism group is a measure of primality.

`DistanceBetweenComplexes` is very inefficient code that attempts to get the distance between complexes by comparing all transformations of their adjacency matrices. This needs work.

`DescendantQ` determines whether a complex is a single barycentric subdivision of another.

`MakeSubdivisionTree` computes the genealogy of a complex in terms of barycentric subdivision.

`DrawSubdivisionTree` draws the family tree generated by the previous function.

`PlotComp` is a primitive plotting routine because it only plots the edges in a complex.

`ComplexPlot` is a plotting routine that shows triangles as well. For large complexes it is difficult to see much.

`DynamicPlot` uses neat new *Mathematica* dynamic updating to help visualize complexes, allowing the user to move vertices out of the way and see what's going on.

## 7 Agenda

- 0) Make some 10-vertex  $g = 3$ .
- 1) Manipulate graphs.
- 2) Tell if 2 triangulations are equivalent by hierarchy of graphs. Test equivalence of known unique minimals. See how many different 8-vertex 1-holers we get.
- 3) Relative frequencies for swaps
- 4) Test for barycentric subdivisions and genealogy.
- 5) 3-manifolds
- 6) Occurrences mean of particular swaps. I.e.  $P(X \rightarrow Y)$  where  $X, Y$  are equiv classes of triangulations.
- 7) Variable-sized universe as it grows or weighting suspends to closeby boundary vertices.
- 8) Trailing off thingy and Poisson modelling–universe-specific.  
[http://en.wikipedia.org/wiki/Poisson\\_distribution](http://en.wikipedia.org/wiki/Poisson_distribution)
- 9) Figure out universe-size dependence of things.
- 10) Figure out why swap chains converge slowly.
- 11) Get prime parents of subdivision and how many generations we are down.
- 12) Size of the automorphism group and rarity/primalty.
- 13) As universe size gets large, it coincides with actual vertex number. (Conjecture)
- 14) Automorphism groups good when rare, parentage good when common.
- 15) Make full triangulation tree
- 16) Full distance between triangulations via skeleton graphs.
- 17) Note that Heawood in [http://www.eg-models.de/models/Surfaces/Polyhedral\\_Surfaces/2006.02.001/\\_direct\\_link.html](http://www.eg-models.de/models/Surfaces/Polyhedral_Surfaces/2006.02.001/_direct_link.html)

$$n \geq \frac{1}{2}(7 + \sqrt{49 - 24\chi(M)})$$

implies that the triangulations in Pippenger-Schleich are not simplicial complexes.

# 8 Triangulations

Enough fluff. Here in order

## 8.1 7-vertex spheres

$t_{0,7;1} = \{3, 3, 4, 4, 5, 5, 6\} = \{\{1, 2, 3\}, \{1, 3, 7\}, \{1, 7, 2\}, \{3, 2, 5\}, \{5, 2, 7\}, \{7, 3, 9\}, \{7, 9, 10\}, \{10, 9, 5\}, \{10, 5, 7\}, \{9, 3, 5\}\}$   
 $t_{0,7;2} = \{3, 4, 4, 4, 5, 5, 5\} = \{\{1, 2, 3\}, \{3, 2, 9\}, \{9, 2, 4\}, \{1, 3, 5\}, \{9, 4, 10\}, \{10, 4, 1\}, \{10, 1, 5\}, \{10, 5, 3\}, \{10, 3, 9\}, \{2, 1, 4\}\}$   
 $t_{0,7;3} = \{3, 3, 4, 4, 4, 6, 6\} = \{\{1, 2, 3\}, \{3, 2, 7\}, \{2, 1, 5\}, \{3, 7, 1\}, \{5, 1, 4\}, \{7, 2, 5\}, \{5, 4, 7\}, \{1, 7, 10\}, \{7, 4, 10\}, \{10, 4, 1\}\}$   
 $t_{0,7;4} = \{3, 3, 3, 5, 5, 5, 6\} = \{\{1, 2, 3\}, \{3, 2, 4\}, \{4, 2, 10\}, \{10, 2, 5\}, \{1, 3, 9\}, \{1, 9, 2\}, \{10, 5, 9\}, \{9, 5, 2\}, \{4, 10, 3\}, \{9, 3, 10\}\}$   
 $t_{0,7;5} = \{4, 4, 4, 4, 4, 5, 5\} = \{\{1, 2, 3\}, \{3, 2, 8\}, \{1, 3, 5\}, \{1, 5, 10\}, \{1, 10, 7\}, \{5, 3, 8\}, \{8, 2, 7\}, \{7, 2, 1\}, \{5, 8, 10\}, \{10, 8, 7\}\}$

## 8.2 8-vertex 1-tori

$t_{1,8;1} = \{\{1, 2, 3\}, \{1, 3, 7\}, \{3, 2, 8\}, \{7, 3, 5\}, \{5, 3, 4\}, \{4, 3, 6\}, \{4, 6, 1\}, \{4, 1, 7\}, \{1, 6, 2\}, \{3, 8, 6\}, \{7, 5, 6\}, \{7, 6, 8\}, \{5, 4, 8\}, \{8, 4, 7\}, \{6, 5, 2\}, \{8, 2, 5\}\}$   
 $t_{1,8;2} = \{\{1, 2, 3\}, \{3, 2, 7\}, \{1, 3, 8\}, \{1, 8, 4\}, \{3, 7, 4\}, \{4, 7, 1\}, \{4, 8, 6\}, \{6, 8, 7\}, \{6, 7, 2\}, \{1, 7, 5\}, \{4, 6, 5\}, \{5, 6, 1\}, \{1, 6, 2\}, \{3, 4, 5\}, \{7, 8, 5\}, \{8, 3, 5\}\}$   
 $t_{1,8;3} = \{\{1, 2, 3\}, \{3, 2, 5\}, \{2, 1, 7\}, \{1, 3, 4\}, \{3, 5, 6\}, \{7, 1, 5\}, \{5, 1, 6\}, \{1, 4, 6\}, \{2, 7, 6\}, \{2, 6, 4\}, \{6, 7, 8\}, \{6, 8, 3\}, \{5, 2, 8\}, \{5, 8, 7\}, \{8, 2, 4\}, \{3, 8, 4\}\}$   
 $t_{1,8;4} = \{\{1, 2, 3\}, \{3, 2, 7\}, \{2, 1, 4\}, \{4, 1, 8\}, \{4, 8, 7\}, \{7, 8, 3\}, \{4, 7, 6\}, \{6, 7, 2\}, \{1, 3, 6\}, \{6, 3, 4\}, \{1, 6, 8\}, \{2, 4, 5\}, \{3, 8, 5\}, \{5, 8, 2\}, \{8, 6, 2\}, \{4, 3, 5\}\}$   
 $t_{1,8;5} = \{\{1, 2, 3\}, \{2, 1, 8\}, \{3, 2, 4\}, \{4, 2, 7\}, \{7, 2, 8\}, \{1, 3, 6\}, \{6, 3, 8\}, \{8, 3, 7\}, \{1, 6, 7\}, \{7, 6, 4\}, \{8, 1, 5\}, \{6, 8, 4\}, \{3, 4, 5\}, \{5, 4, 8\}, \{1, 7, 5\}, \{7, 3, 5\}\}$   
 $t_{1,8;6} = \{\{1, 2, 3\}, \{3, 2, 8\}, \{8, 2, 7\}, \{7, 2, 4\}, \{1, 3, 7\}, \{1, 7, 4\}, \{2, 1, 6\}, \{2, 6, 4\}, \{7, 3, 6\}, \{6, 3, 4\}, \{3, 8, 4\}, \{4, 8, 1\}, \{7, 6, 5\}, \{8, 7, 5\}, \{6, 1, 8\}, \{6, 8, 5\}\}$   
 $t_{1,8;7} = \{\{1, 2, 3\}, \{1, 3, 5\}, \{3, 2, 4\}, \{2, 1, 8\}, \{1, 5, 6\}, \{5, 3, 7\}, \{2, 8, 5\}, \{5, 8, 6\}, \{7, 3, 6\}, \{7, 6, 8\}, \{7, 8, 4\}, \{7, 4, 2\}, \{7, 2, 5\}, \{1, 6, 4\}, \{4, 6, 3\}, \{4, 8, 1\}\}$

## References

- [AJL] <http://arxiv.org/abs/hep-th/0604212> Quantum Grav
- [B] <http://www.expmath.org/expmath/volumes/15/15.3/Banagl.pdf> Banagl
- [BIZ] Bessis, C. Itzykson, and J.-B. Zuber, *Adv. Appl. Math.* 1, 109 (1980)
- [BM] Random Construction of Riemann Surfaces, *J. Differential Geometry*, **68** (2004) 121-157
- [D] <http://arxiv.org/abs/math/0701735> Datta
- [DE] <http://arxiv.org/pdf/math.CO/0504039> Durhuus Eilers
- [DJ] Durhuus, Jonsson, *Remarks on the entropy of 3-manifolds* Nuclear Physics B 445 (1995) 182-192
- [G] Gamburd, A. <http://arxiv.org/pdf/math/0501283>
- [H] <http://www.iop.org/EJ/abstract/0264-9381/2/5/013> Hartle
- [PS] Nicholas Pippenger, Kristin Schleich, Topological characteristics of random triangulated surfaces *Random Structures and Algorithms*, **28**, no. 3, p 247-288 (2006)